Check for updates

ENGINEERING

Grasping and rolling in-plane manipulation using deployable tape spring appendages

Gengzhi He, Curtis Sparks, Nick Gravish*

Copyright © 2025 The Authors, some rights reserved; exclusive licensee American Association for the Advancement of Science. No claim to original U.S. Government Works. Distributed under a Creative Commons Attribution NonCommercial License 4.0 (CC BY-NC).

Rigid robot arms face a tradeoff between their overall reach distance and how compactly they can be collapsed. However, the tradeoff between long reach and small storage volume can be resolved using deployable structures such as tape springs. We developed bidirectional tape spring "fingers" that have large buckling strength compared to single tape springs and that can be spooled into a compact state or unspooled to manipulate objects. We integrate fingers into a robot manipulator that allows for object Grasping and Rolling In Planar configurations (called GRIP-tape). The continuum kinematics of the fingers enables a multitude of manipulation capabilities such as translation, rotation, twisting, and multi-object conveyance. Furthermore, the dual mechanical properties of stiffness and softness in the fingers endow the gripper with inherent safety from collisions and enables soft-contact with objects. Deployable structures such as tape springs offer opportunities for manipulation in cluttered or remote environments.

Downloaded from https://www.science.org at University of California San Diego on April 23, 2025

INTRODUCTION

Robotic manipulators with large reach and small storage volume have substantial potential for operation in remote environments such as space and the deep sea. However, striking a balance between a large manipulation workspace and small storage volume poses a challenging design problem. Traditional rigid-link–based robot arms are fundamentally limited because their physical volume does not change during operation. To circumvent this tradeoff between reach and volume, engineers have looked to deployable structures that can expand in volume from compact to extended states (*1*, *2*). However, current deployable manipulators face a fundamental limitation that the volume changing body and the end-effector are typically separate entities. The end effector thus adds substantial weight to the system, and it requires cabling to be routed through the deployed structure, and because gripping can only occur at one location, the whole system lacks reconfigurability. In this work, we will present a manipulator that uses deployable structural elements as manipulation surfaces leading to a lightweight, extensible mechanism that is able to achieve versatile manipulation capabilities.

Some of the earliest deployable manipulators can be traced back to the kinematic mechanisms of the industrial age and before (*2*). For example, the scissor mechanism may be the simplest example of a linkage system that can substantially increase in length through actuation of a single degree of freedom. Roboticists have leveraged expandable linkages such as the scissor mechanism to create deployable robot arms with gripping end effectors (*3*, *4*). Similarly, concentric tube telescoping structures have also been used to expand robot arms prismatically from a collapsed state (*5*). While scissor and telescoping mechanisms are limited to prismatic motion, more complex planar or spatial linkage arrangements can yield other three-dimensional modes of expansion (*6*–*8*). In addition, kinematic expansion need not be limited to mechanical linkages. For example sheets of folded paper using origami designs can also be deployed from flattened states to form elongated structures (*9*). Origami mechanisms can often be treated similarly to linkage systems, while they present new opportunities for fabrication, control, and stiffness modulation (*10*–*13*). Deployable linkage systems are predominantly made from rigid structures, and thus, they have the benefit of predictable kinematics. However, linkage-based deployable manipulators suffer from the same limitation as traditional robot arms: Their physical volume never changes, and thus, they require careful design to pack the structure into a small volume. To circumvent this limitation, recent advances in deployable robotics have leveraged soft materials that enable volume change through the system's elasticity or flexibility (*14*).

Soft robots composed of compliant materials enable adaptation to the environment during locomotion (*15*–*18*), responsive shape change for grasping complex objects (*19*, *20*), and inherent safety when interacting with or around humans (*21*). A recent design paradigm to make deployable mechanisms in soft robotics is engineered length and volume change of the robot body for robots that "grow." Volumetric growth has been developed in systems such as pneumatic actuators (*22*, *23*), robot skins that enable body eversion (*24*–*28*), flexible zipping structures (*29*, *30*), or additive manufacturing technology (*31*, *32*). Growing robots have thus far shown great promise in deploying over extremely long lengths (*24*), moving through challenging substrates such as sand (*33*) or the body for medical procedures (*34*), and relying on simple off the shelf materials. While soft growing robots are capable of more volume expansion compared to linkage-based mechanisms, they still suffer from the challenge that they must carry a separate end effector for manipulation. This limitation makes cable routing through the expanding body a challenge for soft-bodied deployable robots.

Another category of deployable manipulators is those that use a change in material curvature to collapse/expand and to modulate stiffness. Tubular deployable structures that can be flattened and rolled into a tight coil and extended into a strong linear beam are the most common form of these systems (*1*). In the flattened state, the structure is relatively flexible to bending; however, when the cross section is expanded to a circle (or arc), substantial strength is provided by the bending resistance of curved materials (*35*). Tubular mechanisms often are fabricated from composite material such as carbon fiber or metals such as steel. Tubular-based deployable structures have a long history stemming back to the early days of space exploration and satellite deployment (*2*, *36*). These mechanisms

Department of Mechanical and Aerospace Engineering, University of California San Diego, 9500 Gilman Dr., La Jolla, CA 92093, USA.
*Corresponding author. Email: ngravish@ucsd.edu

have been used as deployable beams (*37–39*) and reconfigurable truss systems (*40*, *41*) for robotic applications.

An exciting recent area of development for deployable manipulation is the use of tape spring–based mechanisms for robotic arms. Tape springs are a special example of a tubular structure that can be easily collapsed flat, they exhibit bistable buckling behavior that can be used for energy storage/release (*42*), and they have anisotropic stiffness for passive compliance. Recent robots have used tape spring appendages with claw and adhesive end effectors to grasp onto cave walls (*43–46*) or to create truss structures and manipulators (*41*, *47–49*). Furthermore, robot arms that use two antagonistic tape springs can form local bends to place grasping anchors in challenging to reach locations (*50*, *51*). The curvature-dependent compliance of tape springs enables joint-link configurations to be reconfigured in robot arms by pinching locations to flatten the curvature (*52*, *53*). Last, small-scale tape springs are being developed for steering needles through tissue (*54*). A common design paradigm of these recent robots is the use of tape springs as a structural element of the robot, whereas environment manipulation occurs through special end effectors.

In this work, we present a concept for deployable manipulation using tape springs in which the deployable structure is also the manipulator surface. With two appendages, the manipulator robot is capable of object Grasping and Rolling In Planar configurations, and we call this robot GRIP-tape (Fig. 1A). Different from previous studies (*43*, *47–49*), we use the entire length of the tape spring as a gripping surface that makes the arms lightweight (no extra motors or mechanisms needed at the end), eliminates any cabling requirements for an end effector, and enables versatile manipulation kinematics such as multi-object conveyance and rotation (Fig. 1B). Furthermore, by developing laminated bidirectional tape springs, GRIP-tape has isotropic bending stiffness in the straight state (Fig. 1C), whereas in the bent state, the tape springs provide high compliance, enabling reconfiguration (Fig. 1, D and E, and movie S1) and the ability to interact with delicate objects. In the following sections of this paper, we will elaborate the design principles for GRIP-tape and demonstrate how using tape springs as deployable manipulators can enable a wide variety of manipulation capabilities.

RESULTS

Design

Development of bidirectional tape spring appendages

The GRIP-tape robot relies on the mechanical properties of curved beams for gripping stiffness and smooth hinge reconfiguration (Fig. 1, D and E). To begin our design of a tape spring gripper, we first sought to analyze the mechanical performance of tape springs to validate that sufficient gripping force could be supported by deployed tape appendages.

Tape configurations. A single tape spring like that found in a tape measure is relatively stiff when loaded by a transverse force pointing into the concave direction of the tape curvature (see movie S1). However, when loaded into the direction of curvature or with torsional moments along the longitudinal axis of the tape, a single tape spring will quickly bend and not be capable of supporting load. To avoid the anisotropic buckling associated with transverse loading

Downloaded from https://www.science.org at University of California San Diego on April 23, 2025

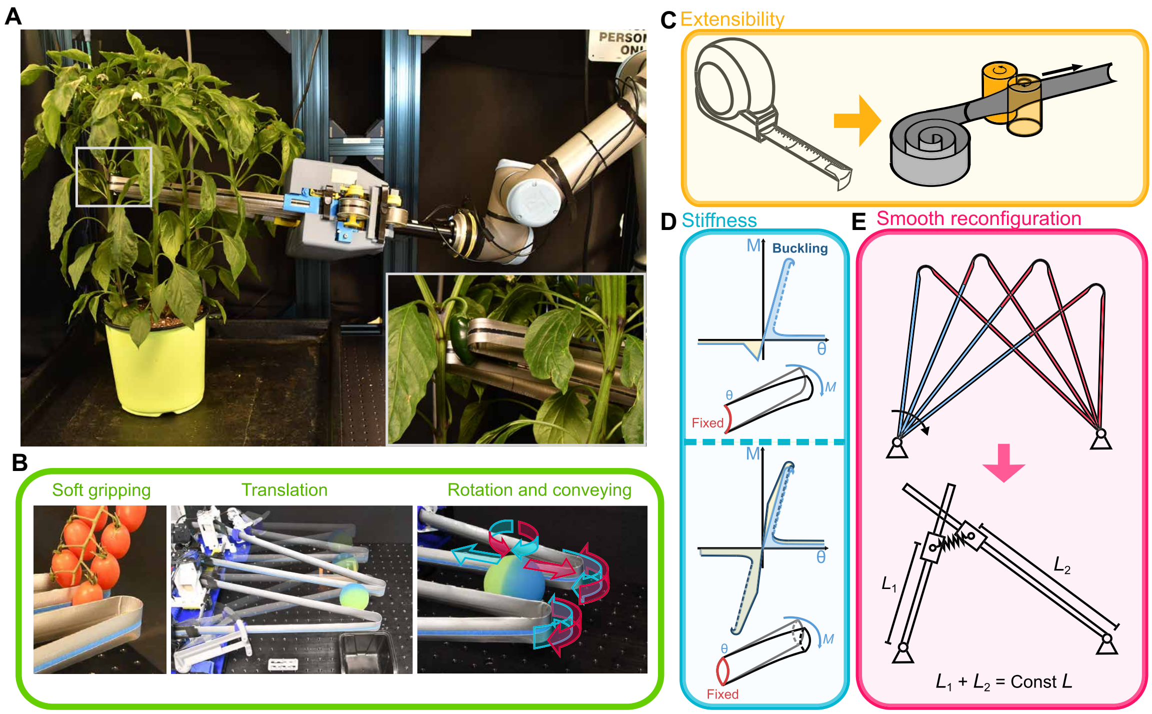

Fig. 1. Functional basis, implementation, and demonstrated capabilities of the deployable gripper GRIP-tape. (**A**) An implementation of the two-digit manipulator on a robot arm. (**B**) Capabilities of the tape spring gripper include the ability to interact with soft objects, translate objects over large distances in a 2D plane, and in-grasp manipulation including rolling and conveying objects. (**C**) Tape spring beams are capable of being rolled into compact spaces and extended over long distances. (**D**) Beam stiffness is asymmetric in the case of unidirectional tape springs and symmetric in bidirectional tape springs. (**E**) By bending the tape spring, a reconfigurable appendage is formed. The kinematics of this appendage is modeled as two rotation-prismatic joints coupled through an elastic spring.

or the twisting failure from torsional loading, we sought to make a symmetric tape spring structure by binding two tape springs together along their length. This "bidirectional" tape design enables the tapes to spool into a compact shape for deployable applications while still retaining the stiffness required for gripping applications. Symmetric shell designs have been previously explored for deployable composite booms (*55*). We fabricated bidirectional tape springs for GRIP-tape by first aligning two spring-steel tape springs collected from an off the shelf tape measure (Fig. 2A). Next, we applied an adhesive layer (duct tape) along the sides of the two tapes to adhere them together.

Three-point bend tests. To compare the strength performance of the bidirectional tape with normal tape springs, we conducted a three-point bending test (see movie S1). The results, as depicted in Fig. 2B, reveal that compared with the two configurations of unidirectional tape, the bidirectional tape exhibits the highest buckling force, indicated by the load peak. In the case of the unidirectional tape loaded on the concave side and forming an equal-sense bend (the green line), the load displacement curve is smooth instead of a drastic drop, implying that the bending failure of the tape is gradual rather than buckling at a force threshold. Because of the geometric relationship inherent in bidirectional tapes, the displacement can be viewed as the combined effect of two unidirectional tapes reacting to the same applied load. In tests involving the unidirectional tape loaded on either the convex (opposite-sense) or concave (equal-sense) sides, it is likely that friction between the test platform and the two edges of the tape due to the flattening of the curve hinders deformation, resulting in an undesired increase in the recorded load. While in the case of the bidirectional tape, the expansion happens between the two tapes simultaneously, and the contact surface and the test platform have almost no displacement, and thus, the friction is reduced.

Bend test with rotary stage. We next measured the buckling force of tapes at various lengths to determine the grip force capabilities of

Downloaded from https://www.science.org at University of California San Diego on April 23, 2025

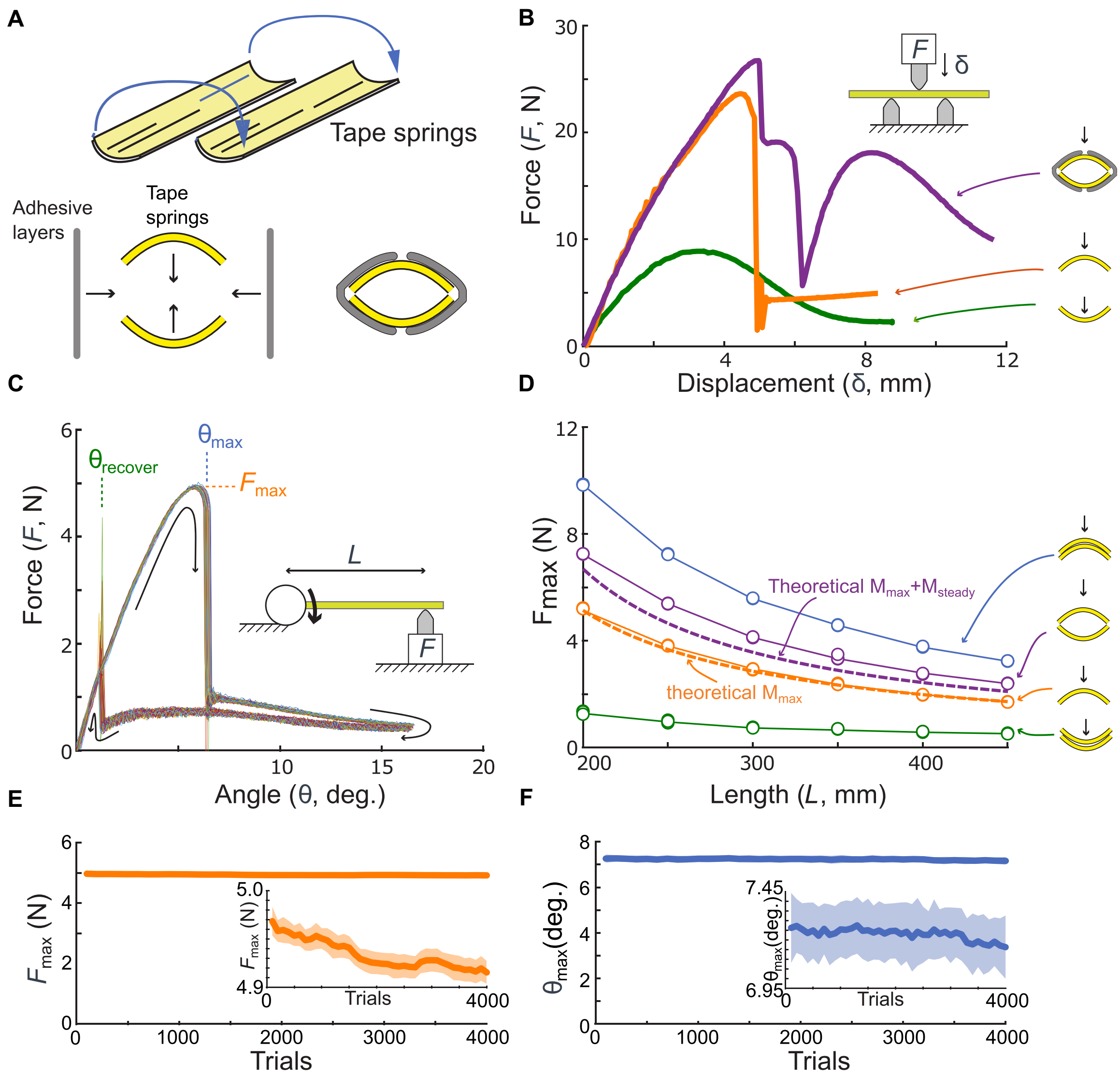

Fig. 2. The buckling force of different configurations of the tape spring and results of the fatigue test. (**A**) Structure of bidirectional tape. (**B**) Results of three-point bend test of different tapes. (**C**) Four thousand cycles of fatigue test. (**D**) Buckling force F_{max} of different setups of tape spring with response to the distance between the fixed point and external force. Dashed lines are theoretical predictions described in text. (**E** and **F**) Trend of the buckling force and buckling angle.

extended tapes. Theoretical modeling of tape spring beams indicates that buckling will occur when a critical bending moment is reached (M_{max}) (*56*), and thus, the grasping force ability of the beams should decrease inversely with length. The experiment consisted of rotating a tape spring beam at the base and measuring the contact force with an object at a prescribed distance from the base until the tape buckles (Fig. 2C). The load cell measures the maximum force that the tape springs exhibit before buckling.

We ran the test on three different configurations of double-layered tape springs: The bidirectional tape and double-stacked tape (two pieces of tape springs stacked in the same direction) loaded in each direction. In addition, a unidirectional tape loaded on its stronger side is also included for comparison. Note that in this test the bidirectional tape was made with a different fabrication method that held the tapes together in a heat-sealed fabric sleeve instead of a duct tape layer. In this fabrication, the tapes are free to move relative to each other and do not have the added stiffness of the duct tape to avoid the influence of the duct tape layer. For each test, the load cell was placed at a distance L from the rotating base, and the tape was rotated into the load cell until it buckled. The peak buckling force was then recorded, and the experiment was repeated three times for each length tested (Fig. 2D).

The results indicate that the opposite-sense buckling force of the double-stacked tape is nearly twice that of the unidirectional tape. However, when unidirectional tapes are subjected to a load into the direction of curvature still only provide minimal force. In contrast, the buckling performance of the bidirectional tape was also good, and this tape can support loads equally on both sides, offering a more versatile and reliable deployable structure for manipulation.

To compare our experimental measurements with the theoretical predictions from thin-shell elasticitiy theory, we implemented the buckling model presented in (*56*). In the Supplementary Materials, we provide details of this model implementation. In the experiment, the tape does not buckle at its very end because the shape of the fastening holder restricts deformation at the end. Accounting for the offset of 75 mm in the buckling location, the theoretical buckling force versus distance curve aligns closely with the experimental data (dashed curve, Fig. 2D).

For the bidirectional tape, the theory requires a slight modification because we do not know how much moment the equal-sense bending contributes during the buckling of bidirectional tapes. As a lower bound on this prediction, we treat the buckling moment as the sum of the opposite-sense buckling moment M_{+}^{max} and the steady moment M^* to represent the total moment (see the Supplementary Materials). The steady moment M^* represents the minimum value of equal-sense bending, meaning the actual contribution of equal-sense bending is certainly greater than this value. This slight underestimation of the moment contributes to the gap between the theoretical and experimental data (dashed curve, Fig. 2D). Another possible source of this discrepancy is the sliding friction between the tapes as buckling occurs, which would increase the actual buckling force compared with theory. For the subsequent analysis of the maximum gripping force that can be applied at different tape lengths, we rely on the theoretical curve as it establishes a conservative lower bound for gripping force.

Fatigue and max buckling force. An important feature of a gripper is the capability to durably operate over long periods of time. This is potentially problematic for soft robots and deployable systems where the structures of the robot will undergo large deformation and strain. Specifically for the GRIP-tape robot, we require that the tape spring appendages roll and unroll repeatedly during operation without fatigue and not exhibit failure from errant collisions that cause them to buckle. To test the fatigue performance of our bidirectional laminated tape springs, we performed a test to measure the buckling force and angle over repeated loading. Using the same setup as the buckling test, we mounted a load cell on a track 20 cm away from the starting point of the tape spring. During the rotation, the tape measure contacts the load cell, buckles, stops at 16.5°, and rotates back to the initial position. We gathered the data of 4000 cycles from the load cell measuring the maximum forces before buckling (Fig. 2E) and the angle at which the tape spring buckles (Fig. 2F). After 4000 trials, the buckling angle and buckling force decreased minimally. The buckling angle reduced from 1.28° to 1.16°, and the buckling force reduced from 4.97 to 4.92 N. In the size and force range of GRIP-tape, such an amount of variation is acceptable.

Kinematics and control

GRIP-tape appendages. We designed GRIP-tape to use two triangular-shaped appendages as the left and right gripping surfaces (Fig. 3, A and B), each consisting of bidirectional tape. Learning from the theoretical analysis, the performance of the gripper is influenced by the transversal curvature and the number of tape layers, which directly affect the buckling moment and tip stiffness. Increasing either thickness or curvature would increase the gripping force by improving stiffness and buckling resistance; however, this would reduce the flexibility of the tapes limiting their "safety" when inadvertently colliding with obstacles. To optimize performance, we selected a single-layer configuration for each side, balancing stiffness and gripping force. Thus, the design incorporates an inherent safety feature, with the tape buckling at a specific load threshold to prevent excessive forces that could damage the gripper or the object.

The straight sections of the appendages act as structural elements that are capable of supporting transverse and compressive loads, whereas the buckled end of the appendage is a rolling hinge that can change the overall shape of the appendage. The inner sides of the two appendages are the gripping surfaces, and our design facilitates object grasping anywhere along the inner length of the appendages. Each appendage has three independent control inputs (Fig. 3, B and C): control of the outer beam angle (θ_1) and control of the length change from either the outer or inner side of the appendage (δL_1 and δL_2, respectively). The inner beam angle is free to rotate and is determined by the total tape length L and outer angle θ_1. Both left and right appendages have control over θ_1 and tape length change and thus can be controlled individually. Last, a single motor controls the symmetric gap width between the inner tapes w. The combination of three independent control inputs on the left and right appendage, and the width control yields seven overall control variables to position the tapes.

Individual actuation of the appendage control inputs leads to four primary modes of appendage shape control (Fig. 3C). By changing the length of either the inner or outer section ($\delta L_1 \neq 0$ or $\delta L_2 \neq 0$), the outer beam will remain at angle θ_1, while the overall tape length shortens, causing the inner beam to bend. Note that the δL_1 and δL_2 actuators only control the relative change in tape length, while the respective side lengths of the triangular-shaped appendage are determined by the overall tape length and side angle θ_1. By changing the outer section angle θ_1, the appendage traces a sweeping motion across the workspace. If the overall tape length is held constant, then the tip will trace out an elliptical shape. Changing the tape width w

Downloaded from https://www.science.org at University of California San Diego on April 23, 2025

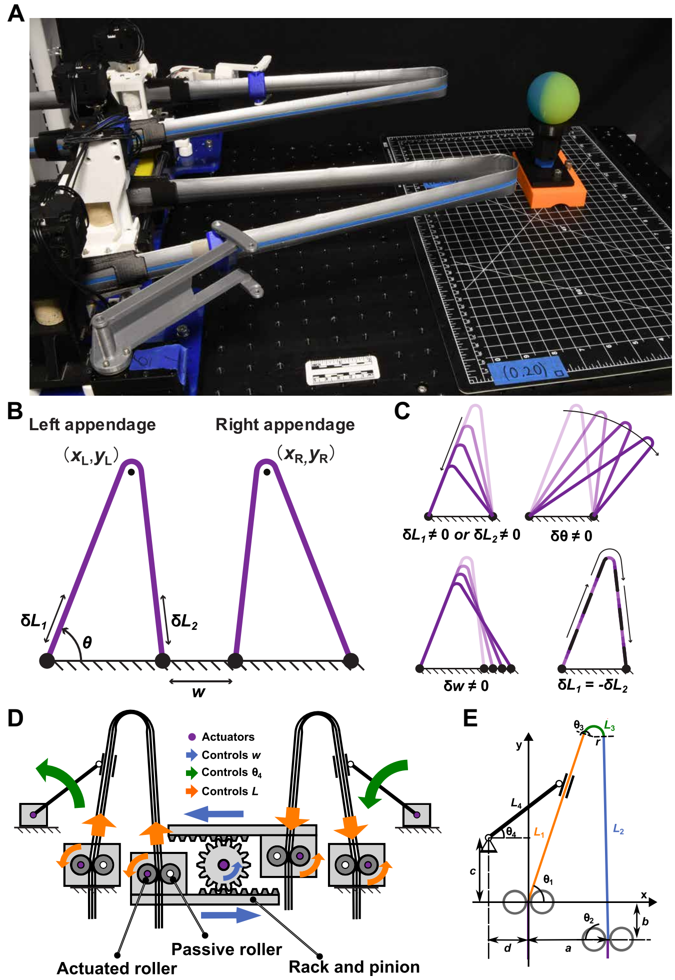

Fig. 3. Kinematics and design of the GRIP-tape manipulator. (**A**) Planer test platform for GRIP-tape. (**B**) GRIP-tape is composed of a left and right digit. Each digit has independent control over the tip location denoted by the black dots. (**C**) Four insets show the basic modes of appendage control. (**D**) Schematic of the overall control inputs for the two tape spring appendages. (**E**) Representative model of the left appendage with actuation inputs from two roller units (θ_1, θ_2) that control the left-right length of the appendage and a rotational input (θ_4) that controls the angle of the appendage.

results in a change of the inner section angle and side length, while the outer tape remains at a fixed angle θ_1. Last, an equal rate of tape unspooling and retraction on the inner and outer sections ($\delta L_1 = -\delta L_2$) results in a motion where the overall shape of the appendage is unchanged, but the surface motion of the gripper will either move inward or outward which can be used for object rotation or conveyance.

Mechanism design and workspace. The GRIP-tape robot is actuated by a total of seven independent motors as depicted in Fig. 3D. For each appendage, two motors are dedicated to controlling the length change of the inner and outer tape spring beams, and one motor controls the outer angle of each appendage. The exact layout and dimensions are presented in materials and methods and Fig. S1A. The last motor is used for adjusting the inner width between the appendages, w. This adjustment is achieved through a rack and pinion mechanism (refer to Materials and Methods and fig. S1B).

One tape extruder assembly consists of two 3D printed cases, each housing a roller. One of the rollers is driven by a servo motor and is equipped with sandpaper to enhance friction, while the other roller is passive and freely rotates. The rollers are pressed tightly together, and the bidirectional tape is passed between them. Supporting guides hold the tapes in position on both sides of the rollers (refer to Materials and Methods and fig. S1, C and D). For the length of an appendage, both extruders are only capable of controlling the total length L, and the overall appendage's length (shape) is also influenced by the distance between the two extruders a and the orientation of the angular control beam θ_4 (refer to Fig. 3E). The appendage's angular orientation is governed by a guiding ring covered by low-friction material and an angular control beam located on each side (refer to materials and methods and Fig. S1E). The pivot axis of the angular control beam is affixed to a servo motor mounted on the base, and so the outer mounting geometry of the appendages (lengths c and d in Fig. 3D) is predetermined and not adjustable. Conversely, the triangle base width (parameter a in Fig. 3D) for each appendage can be changed and thus is designed to facilitate the grip and conveyance of objects of varying sizes. Notably, because the racks are mounted parallel to the x axis, parameter b is set and not adjustable.

The gripping workspace is determined by the combined range of motion of the appendages, each with an angle restricted annular reach (Fig. 4A). For the left appendage, the left angle boundary is constrained by the tape coming into contact with the pivot of the angular control beam. The right boundary is limited by the angular control beam colliding with the extruders. In the radial direction, the inner workspace radius is defined by the minimum allowable length of the appendage to ensure that the tip does not interfere with the angular control beam. The outer workspace radius is determined by the allowable extension distance of each tape before they buckle under their own weight. The right appendage workspace is the mirror of the left and the total workspace is the inclusive combination of the left–right.

Figure 4B shows an image of the total workspace of the gripper. We generated a heatmap illustrating the maximum grip force that the GRIP-tape can sustain at different locations (Fig. 4B). The maximum gripping force was calculated by combining the data from the bend test with rotary stage and the workspace analysis. The calculation of the maximum gripping force involves the relationship between the maximum force resisting bending and the deployed length (i.e., the distance between the guiding ring where the buckling of appendages happens and the rolling joint) of the supporting side of the appendage (Fig. 2D). Besides bending, another potential failure mode is torsional bending under load. For instance, in horizontal gripping, a heavy object could cause the inner sections of the appendage start to rotate torsionally downward. Our experiments indicate that the tapes are able to support larger weights at larger distances (i.e., larger torsional failure moments) than they are capable of generating gripping forces. This means that even if the friction coefficient between the object and the appendage is large, the torsional load the appendages can support is still greater than the weight that the maximum gripping force can hold. As a result, bending buckling becomes the dominant failure mode during grasping.

Although tape appendages are capable of interacting with objects along their inner surfaces, due to the convenience of directly controlling the location of the appendage's tip, we use the minimum length of the appendage to calculate gripping force. This heatmap

Downloaded from https://www.science.org at University of California San Diego on April 23, 2025

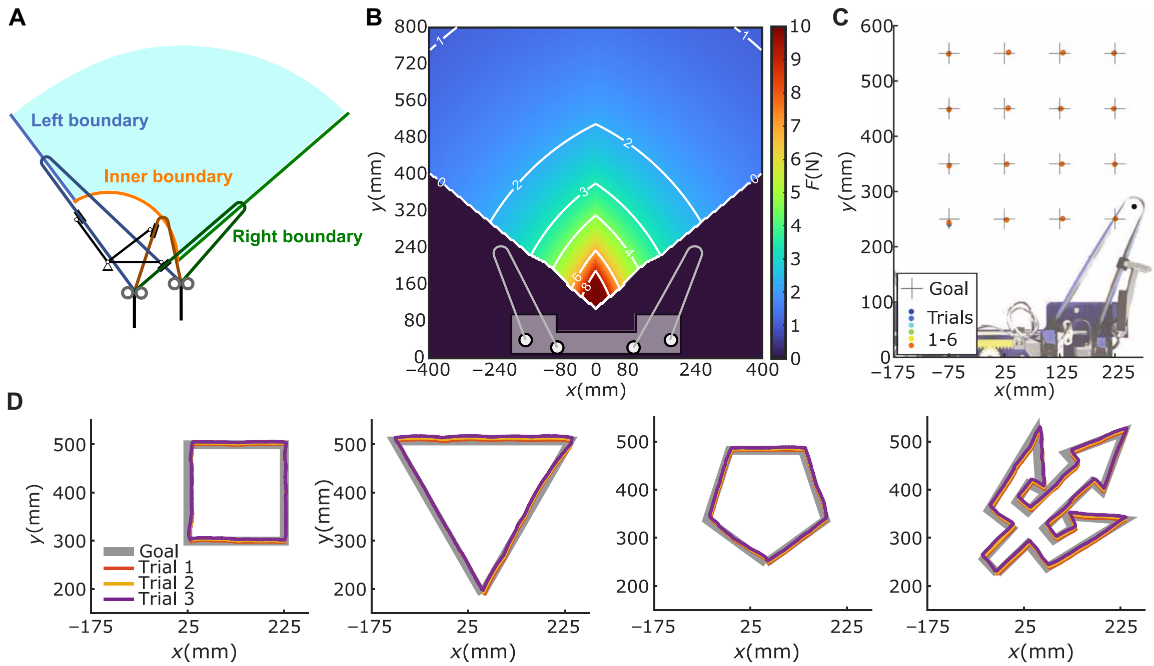

Fig. 4. Demonstration of GRIP-tape appendage kinematics. (**A**) Workspace of the left appendage. (**B**) Combined workspace of both appendages with the maximum gripping force computed from buckling measurements and indicated with a color map. (**C**) Inverse kinematics position error of the right digit tip location from over six trials. (**D**) Results from right digit tip location tracing over three trials with four different shapes. See movie S3 for the video.

reveals that the GRIP-tape can support the highest gripping force near the base, particularly in the central region. As the distance from the base increases and the location moves laterally away from the central line (i.e., $x = 0$ mm), the gripping force diminishes.

Inverse kinematics and forward kinematics. To derive the forward and inverse kinematics, we assume that an appendage is separated into three sections: (i and ii) Two straight line sections L_1 and L_2, and (iii) a constant curvature arc of length L_3 that is tangent to both L_1 and L_2 (Fig. 3D). Although the deployed beams of tape still experience some deformation when load is applied, to simplify the model, we assume that they are rigid links. In our design, b, c, d, and L_4 are known and constant variables. Because r reflects the load on the appendage, in a scenario with almost 0 load, we use a constant $r = 15$mm, which is determined from measurements.

By inputting (x, y) and a, the inverse kinematics solves for the length of each section L_1, L_2, L_3, and θ_4. The inverse kinematics purely involves a geometric calculation. The main steps of inverse kinematics involve determining lengths and angles of the supporting contact section L_1, L_2, θ_1, and θ_2 with the desired x, y position as the first steps. With the relationship $\theta_1 - \theta_3 = -\theta_2$ and known variable r, the length of bending section L_3 is derived. Within the workspace, θ_4 can be bijectively mapped from θ_1.

The forward kinematics use inputs of total length L, arm angle θ_4, and the horizontal distance between the extruders a to solve for the location of the center of the rolling joint (x, y). The location of the outer extruder is set as the origin. The location of the guiding ring on the angle control arm relative to the origin is $\mathbf{v} = \begin{bmatrix} -d \\ c \end{bmatrix} + L_4 \begin{bmatrix} \cos(\theta_4) \\ \sin(\theta_4) \end{bmatrix}$. The appendage angle (θ_1) is determined by the unit vector of the guiding ring position $\hat{\mathbf{v}} = \mathbf{v} / |\mathbf{v}|$. The center of the rolling joint can be found through a vector sum of the outer appendage arm and a perpendicular radius of the curve r; $X = L_1\hat{\mathbf{v}} + r\begin{bmatrix} 0 & 1 \\ -1 & 0 \end{bmatrix}\hat{\mathbf{v}}$. The length of the outer appendage arm L_1 is found by solving three nonlinear constraint equations. Two equations come from the x and y vector sum of the two appendage arms and their perpendicular radius, as both arms of the appendage must meet at the center of the rolling joint. The final equation is the total length constraint, as the total length of the appendage L is known

$$L = L_1 + L_2 + r(\theta_1 - \theta_2 + \pi)$$

$$L_1 \sin(\theta_1) + r\sin(\theta_1 - \pi/2) = L_2 \sin(\theta_2) + r\sin(\theta_2 + \pi/2) - b$$

$$L_1 \cos(\theta_1) + r\cos(\theta_1 - \pi/2) = L_2 \cos(\theta_2) + r\cos(\theta_2 + \pi/2) + a$$

Both inverse and forward kinematics are presented in the Supplementary Materials and fig. S2.

To validate the kinematics model of the GRIP-tape appendage, we performed two experiments to monitor positioning accuracy and repeatability. In the first experiment, we commanded the appendage to move to 16 target points in the workspace, repeating this over six trials (Fig. 4C). Across the six trials for each of the 16 target points, the norm of the vector distance between the desired x-y location and the measured x-y location was determined to be an average position error of 3.72 ± 0.35 mm. This means that the mean absolute error of the 96 sample points in the plane is 3.723 mm. The mean of SDs of the error is 0.3548 mm. The mean was likely not centered at zero because of possible oversimplifications of the inverse kinematics model. These oversimplifications would include: imperfection in the fabrication of the tape and mechanism, inaccurate representation of

Downloaded from https://www.science.org at University of California San Diego on April 23, 2025

the tape thickness, inaccurate assumption in the kinematic model, potential vertical sag of the tape, and deviations of the bend curvature due to internal stress from the tape. To demonstrate the motion control capabilities from the GRIP-tape kinematics, we conducted a second set of experiments in which we moved the appendage tip along a variety of path shapes (Fig. 4D). Path following was tested through three cycles of path following across four polygonal shapes. The motion paths were repeated consecutively without any calibration between. We observed good tracking behavior between the desired and observed paths (Fig. 4D and movie. S3) indicating that GRIP-tape is capable of suitable positioning control.

Appendage mechanics

Bidirectional tape extensibility. In each appendage of the GRIP-tape, two tape extruders adjust the length of the appendage. By extending or retracting tape with the extruders, the overall length and reach of the appendage can be changed. To determine how far an appendage can reach, the GRIP-tape was mounted horizontally, and a tape appendage was extended parallel to the floor until it buckled under its own weight. This was done with both a unidirectional tape appendage and a bidirectional tape appendage. The longest successful extension of a unidirectional tape appendage reached was 1.07 m. Because of gravity, oscillation, imperfections in fabrication, and the anisotropy of the unidirectional tape, it buckles on itself and collapses. A bend is formed diagonally across the tape spring that causes the end of the appendage to hang down toward the floor. The bidirectional tape does not have the same anisotropy, so it performed much better. The bidirectional tape successfully extended to a max length of 1.52 m. Unlike the unidirectional tape, the bidirectional tape is limited primarily by weight and the stiffness of 3D printed parts. As the bidirectional appendage reached out farther, it began to sag under its own weight and caused bending in the base and extruder assembly as well.

To reach high extensions of the appendage while maintaining a small size, it is necessary to store long lengths of the tape springs in a small volume. When used in a tape measure, tape springs are stored in a compact form by winding them on a spring-loaded spool. This can also be done for the unidirectional tape by wrapping both sides of the appendage tape around a spool on the opposite side of the extruders. However, bidirectional tapes are not capable of this. The two tapes inside the wrapping are unable to slide (shear) relative to each other. When the tape is wrapped around a spool, there is a mismatch in the length of material needed for the tape on the inside of the coil and the tape on the outside of the coil. This causes the bidirectional tape to form bumps and kinks as the length mismatch builds up. These imperfections prevent even coiling of the tape. To address this issue, our solution is to bind the two tapes with a low-friction sleeve between the adhesive and the inner tapes. Because the adhesive is not directly attached to the tapes, they can slide internally with respect to each other and prevent the problematic accumulation of shear strain along the tape length (movie S2). By adding an external sleeve to the bidirectional tape fabrication process, we are able to spool up the appendage tape and unroll it during deployment.

Soft-contact object interaction through hinge serial compliance. The structure of one appendage of the GRIP-tape can be represented kinematically as two prismatic links, with constant length constraint, that are connected by a nonlinear spring at the tip of the appendage (Fig. 1E). As GRIP-tape interacts with an object the bend curvature at the end of the tape appendage undergoes changes corresponding to the change in gripping force. As the gripping force increases, the radius of curvature decreases, leading to a spring-like resistance. To quantify this resistance, different configurations of tape were bent 180°, and the tapes were subjected to compression tests. The force readings during the compression of the tape were recorded as a function of displacement, enabling the measurement of the "stiffness" in the tape's contact mechanics (fig. S3A). These results were compared with a theoretical curve derived by differentiating the strain energy U of the bending section, as given in (*57*)

$$U = \frac{Db\psi}{2}\left(\frac{1}{r} + \frac{r}{R^2} - \frac{2\nu}{R}\right)$$

with respect to the displacement d. The strain energy is minimized when $r = R$, indicating that the radius of curvature without applied pressure is R, leading to $d = 2(R - r)$. In this expression, ψ is the bending angle, which is 180° in our case, and b is the tape's width, defined as θR.

By fitting the experimental data to a polynomial curve (see the Supplementary Materials), we derived the experimental relationship between the applied load and the deformation of the spring-like bending. The observed discrepancy between the theoretical and experimental curves highlights the role of deformation in the transition region—the segment that connects the bent arc to the straight section. This deformation is not accounted for in the theoretical model. Based on our observations, assuming the length of the transition region remains constant during compression, the following phenomena occur: As the arc is compressed, the bending region shortens, while the straight region lengthens by the same amount. This redistribution reduces the potential energy associated with the lengthened straight region, thereby diminishing the overall energy gained during compression. Consequently, the experimental results indicate an effective material stiffness that is lower than the theoretical prediction.

As a means of comparison to other elastomeric soft grippers, we envisioned that the tape spring bend joint is a 15 mm–by–25.4 mm–by–30 mm sized cube and calculated an effective Young's modulus of this mechanism. Comparison of the approximate Young's modulus of the tape spring bend with other soft materials in fig. S3D indicates that the contact interaction mechanics performance is broadly similar to silicone elastomers.

Grasping capabilities and demonstrations

In the prior section, we demonstrated the unique mechanics of deployable tapes and our ability to exert simple kinematic control over the appendages. We now illustrate the gripping capabilities of the two appendage GRIP-tape system.

Gripping, translating, and rotating objects

Once both appendages of the GRIP-tape contact the target object with a sufficient load, a grasp is formed, and we can translate the object by simultaneously moving the left and right appendages to different target positions. In our first demonstration, we grasp a rubber ball at the tip of the appendages, translate the ball to a desired position, rotate the ball in place, and then convey the ball toward the gripper base and release it into a bin (movie S3). The GRIP-tape is capable of grabbing objects of varied shapes and stiffnesses such as individual tomatoes and an entire tomato vine (Fig. 5A and movie S4).

In-place, continuous rotation is a unique capability of the GRIP-tape kinematics. Object rotation is achieved by displacing the object contact points in opposite directions (movie S3). The overall length of the appendage can be kept constant during rotation by spooling

Downloaded from https://www.science.org at University of California San Diego on April 23, 2025

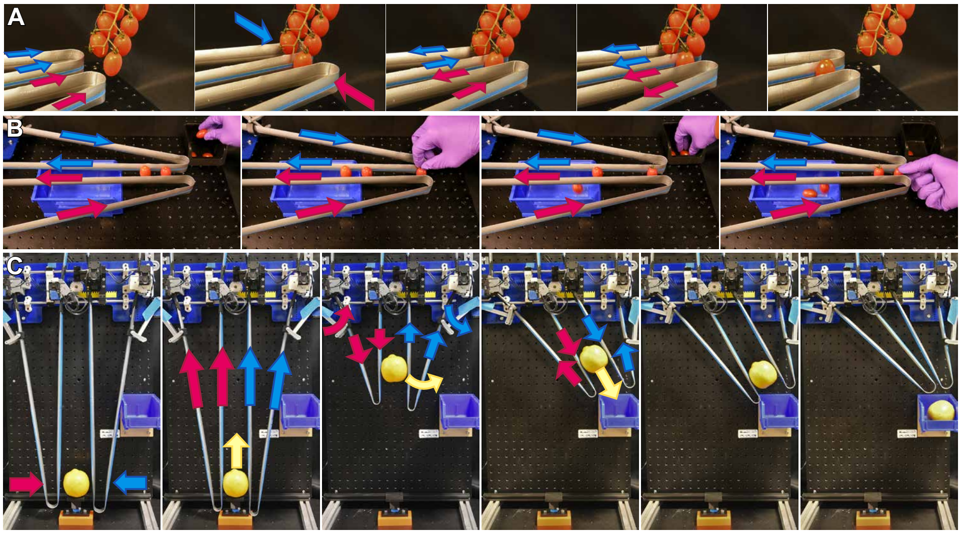

Fig. 5. Demonstrations of basic applications. (**A**) Demonstration of soft gripping and twisting. (**B**) Demonstration of object conveyance. (**C**) Demonstration of lifting.

and unspooling at the base of each appendage. Thus, if we want to rotate a ball of a radius r by 90°, the surface on the contact section of the tape of the left appendage has to extend $\pi r / 2$. To keep the ball at a constant location, the contact section of the tape of the right appendage has to retract $\pi r / 2$. Accordingly, the supporting section of the left appendage retracts $\pi r / 2$, and the supporting section of the right appendage extends $\pi r / 2$.

In-place rotation can be used to accomplish challenging picking operations such as twisting a tomato off of the vine (Fig. 5A and movie S4). The soft-contact capabilities of the tape allow for applying light pressure to the tomato surface, and a continuous in-place rotation twists the tomato, releasing it from the vine. An additional function of GRIP-tape is the capability to convey objects inward to the base while keeping the overall shape constant. Object conveyance can even be extended to multi-object conveyance where several objects can be grasped and simultaneously translated back to the base of the gripper (Fig. 5B and movie S4).

In Fig. 5C, we show a lifting example of grasping a fresh lemon from a distance of approximately 50 cm, vertically lifting the lemon and orienting it over a bin, and conveying the lemon into the bin. In movie S4, we show several other examples of object manipulation including grabbing, translating, and screwing in a light bulb. All demonstrations are performed through teleoperating the robot with a custom-designed app that enables joystick control (fig. S7 and movie S4).

Passive compliance and robustness

The passive compliance of the tape appendage gives it unique capabilities for interacting with objects. For example, if there is an obstacle impeding the planned trajectory, then the appendage is capable of deforming around the obstacle and continuing on its way to reach the desired ending position (fig. S6A and movie S5). If there is a known obstacle in the way that would prevent the appendage from reaching the target normally, then the appendage can deform against the known obstacle and remain capable of grabbing and conveying the target object. Figure S6B and movie S5 show an application of object grasping and conveyance while the appendages are deformed from contact with a wall.

The material properties of spring-steel and the cross-sectional curvature of the tape provide tape springs the robust ability for self-recoverability. A tape spring bent out of its original shape will snap back to its original configuration when released. The GRIP-tape appendages self-recoverability property is demonstrated in movie S5. The appendage is struck while trying to complete a task. The strike causes the appendage to buckle. However, the appendage made of bidirectional tape rapidly rebounds and successfully completes the task.

Force sensing

To allow for force feedback from the GRIP-tape, a load cell was built into the angular control arm (Fig. 6A). Assuming the moments on each section of the appendage are balanced, and knowing θ_4, a, and L, we can derive θ_1, θ_2, L_1, L_1', and L_2 by forward kinematics (refer to Fig. 6B). The relationship between the force on the contact section and the read of the load cell is

$$F_2' = \left(\left\{\left[F_{\mathrm{read}} L_1' / \cos(\theta_1 - \theta_4) + \tau_1\right] / L_1\right\} L_2 + \tau_2\right) / L_2'$$

F_{read} is the reading of the load cell, and τ_1 and τ_2 represent the internal bending torque of the tape spring. To obtain τ_1 and τ_2 at different angles, we measured the internal torque with a bidirectional tape with a pinched point by bending it around this point to a set of different angles. By curve-fitting these data with a spline (fig. S8), we developed a relationship between the bending angle and τ. To demonstrate the force sensing accuracy, we placed another load cell at the tip of the appendage with $L_2' = L_2$, and we compared the force prediction from the base load cell with the actual contact force measured by the contact load cell. An example of the comparison between the real force on the tip of the appendage measured by the additional load cell and the calculated value F_2 derived from the force reading F_{read} on the base is shown in Fig. 6C, demonstrating a very good agreement.

Automatic gripping

The length of appendages and the force feedback in the GRIP-tape allow for locating the position of an object by searching with the appendages and grasping it autonomously. We designed several motion steps to complete automatic gripping (Fig. 6D and movie S6).

Downloaded from https://www.science.org at University of California San Diego on April 23, 2025

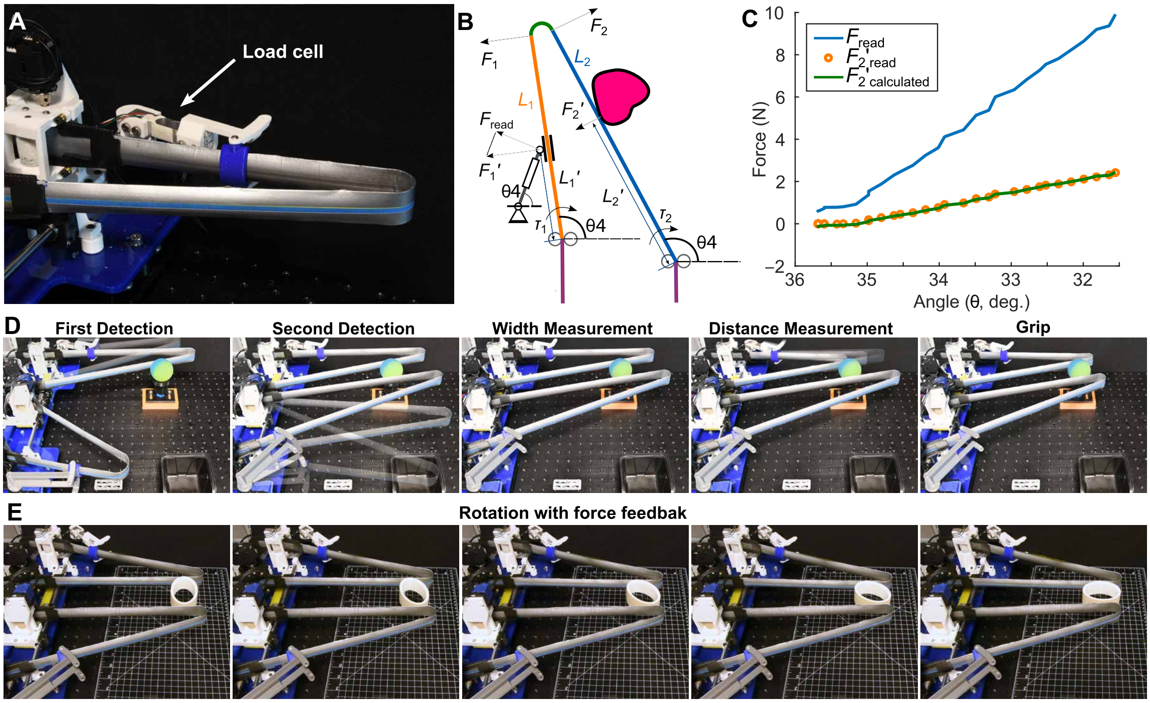

Fig. 6. Force sensing and automatic searching, testing, and gripping. (**A**) Load cell on the angular control beam. (**B**) Balance of moment. (**C**) Comparison of calculated and actual force versus angle of θ_4. (**D**) Automatic detection, measurement, and gripping. (**E**) Object Rotation with force feedback.

In step 1 (fig. S9A) and step 2 (fig. S9B), we locate the object with the left and right appendages by sweeping first the left appendage inward until the contact is detected (force reading exceeds the threshold), and then the right appendage is swept inward until the contact is detected. The steps end when an increase of the force estimate of the F_2 is detected with a contact detection threshold value of 0.25 N. After steps 1 to 2, the left and right appendages are both in contact with the object with a small amount of gripping force. The shapes of the appendages define a gripping axis (the magenta line in fig. S9B) along which the object is located by connecting the origin and the midpoint between the two coordinates of the appendages' tip. However, we have not yet determined the size of the object or the distance of the object along this center line. In some cases, for instance, the friction between the appendage and the object is low, the width of the object can influence the gripping because the angle between the appendages is larger than the self-locking angle so the object could fall out of grip no matter how large the gripping force is. The other reason to measure the width is to fulfill the requirement of conveyance that the contact section of appendages must be parallel. For step 3 (fig. S9C) and step 4 (fig. S9D), the GRIP-tape separates its appendages and reconfigures the contact sections to be parallel to the gripping axis, and then the tapes are moved closer to each other while keeping the paralleled configuration until contact is once again detected by the force sensor. This measurement step now provides the width of the object w, which is the gap between the paralleled contact section of the appendages. Last, to determine the object distance along the grip axis, we retract the left appendage until contact is lost (measured by a sudden decrease in force from the force sensor). Once contact is lost, we mark the gap between the origin and the intersection point of the perpendicular drawn from the tip location of the left appendage to the gripping axis as the shortest distance d', and the distance between the object and the origin is assumed to be the sum of half of the width w and the shortest distance d' (fig. S9E). Once the object location has been determined in the workspace, we can move the two appendages to the sides of the location of the object, form a grasp, and move the object to the desired location (fig. S9F and movie. S6).

Rotation with feedback control

Force feedback also enables the GRIP-tape system to provide closed-loop contact force control. This can be useful, for example, in cases where a nonround object needs to be rotated. Round objects can be rolled in the grip by simply moving the surfaces of the appendage in opposite directions. The object roundness results in a constant grip force while the object rotates (since the cross-sectional width of the object is not changing between the grip points).

While this open-loop rotation works well for round objects, objects of unknown or irregular shape pose a challenge for rotation in a grasp. The softness of the appendage tip can accommodate some small deviations in grip width variation. However, excessive width changes during rotation can lead to either loss of grip (movie. S7), buckling of the appendage, or slipping of tapes inside the tape extruder due to increased gripping force and excessive friction between the tapes and the guiding ring.

To address this issue, we implemented force feedback from the contact force sensor to achieve and maintain a desired gripping force during nonround object rotation. The feedback control adjusts the lateral spacing between the appendages to keep the desired force contact force constant. The force controller is a simple control loop in which the contact force error is used in a proportional controller to servo the grip width. If the force reading is less than the desired force, then the grip width between the appendage ends is decreased. If the force reading is higher than the desired force, then the grip

Downloaded from https://www.science.org at University of California San Diego on April 23, 2025

width distance between the end points is increased. Implementing this force feedback control allows for successful, controlled rotation of elliptical and other nonconstant grip width objects. We compared the performance with and without force feedback by rotating an ellipse and demonstrate that open-loop rotation causes the object to be dropped, while closed-loop force feedback rotation successfully maintains a grasp during rotation. A demonstration of these capabilities is presented in Fig. 6J and movie S7.

Applications of GRIP-tape as an end-effector

After the functions and applications were verified on the planer platform, we designed a more compact GRIP-tape that could be used as an end effector on a robot arm and aims to handle object sizes similar to those that human hands can handle. The robot arm helps to enlarge the workspace from planar to 3D in the applications of GRIP-tape. The system retains the same design and kinematics of the planar test platform while being implemented in a smaller package with integrated tape spools into its main body.

Design of the GRIP-tape end-effector

The design principle is the same as that of the planar test platform, with both using four actuators to control the length of a pair of extendable tape appendages. Adjustments for the smaller-sized design include combining the angular control link with the guide of the outer extruder, swapping the width control mechanism from a rack-and-pinion system to a timing belt, and integrating the spool. For detailed CAD drawings, refer to fig. S10 and movie S8.

Demonstration of manipulation in 3D space

With an end effector–sized gripper, the robot arm expands its capabilities from planar to 3D operations. Leveraging the added degrees of freedom, we replicated the tomato twisting and picking demonstration with a larger tomato, achieving a more accurate and secure picking and dropping (Fig. 7A). Furthermore, we used the end effector to do multistep manipulation tasks such as a combination of object rotation about the z axis (untwisting a cap) and rotation about the x axis enabled by the robot arm (Fig. 7B). In Fig. 7C, we illustrate a potential application of the GRIP-tape end effector by reaching through the leaves of a plant, grasping a pepper, and then twisting the pepper off the stem and pulling it from a plant. The arm enables the precise targeting of the GRIP-tape appendages, while the deployable action of the tape spring finger allows for reaching and manipulating the object. Last, Fig. 7D showcases the combination of the tape appendages' extensibility and the z-axis degree of freedom by reaching into a narrow gap and moving an object from one layer to another through the small gap. Videos of the demonstrations can be found in movie S8.

DISCUSSION

In this work, we have presented the design and testing of GRIP-tape, a soft robotic gripper constructed from tape springs that is capable of object Grasping and Rolling In Plane (GRIP-tape). The GRIP-tape has many of the same advantages as other soft robot grippers, with compliance allowing for interaction with unknown or complex objects (*58*), being inherently safe for human interaction (*21*), and being able to reconfigure its own shape (*59*). The tape appendage mechanism keeps the beneficial properties of robot compliance while also adding additional capabilities for simple in-hand rotation and high extensibility. Thanks to the features of tape springs, the inherent maximum load and self-recoverability of tape appendages provide safety during interaction and ensure robustness in gripping applications. Owing to the continuity and consistency of the tape appendage, the rolling mechanism allows for the seamless renewal of material if any part is permanently damaged during operation, eliminating the need for complicated manual operations. In addition, because of its geometrically defined shape, the tape appendages can be precisely controlled. These key features make the GRIP-tape a versatile system, well-suited for a variety of applications encompassing object gripping, dual modes of translation/rotation, and multi-object conveyance.

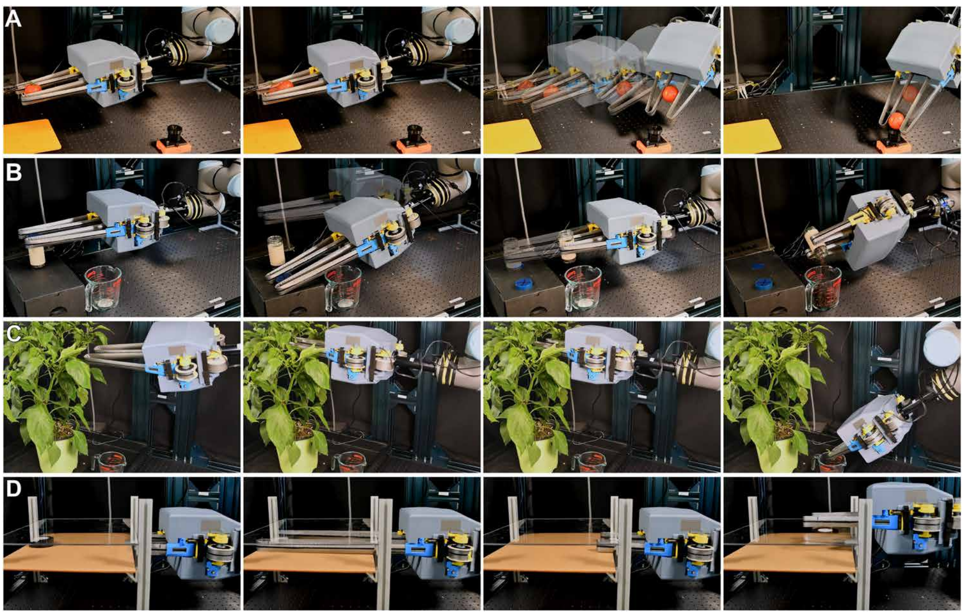

Fig. 7. Manipulation in 3D space capabilities. (**A**) Demonstration of harvesting a fresh tomato by twisting. (**B**) Demonstration of opening and pouring a pepper canister. (**C**) Demonstration of harvesting jalapeño on a plant by twisting and pulling. (**D**) Demonstration of reaching through a small gap.

Downloaded from https://www.science.org at University of California San Diego on April 23, 2025

An enabling capability of the GRIP-tape is the ability to rotate objects in place while in a grasp. Prior grippers have been developed with similar capabilities; however, they have relied on the integration of active surfaces such as conveyor belts mounted onto a traditional gripper. For example, the underactuated modular finger featuring a pull-in mechanism (*60*) and the sheet-based Gripper (*61*) both used driven belts as the contact surface of each finger, aimed at pulling in and gripping, refining the object-picking process. Other examples of active surfaces include Velvet Fingers (*62*, *63*) and an active surface gripper consisting of an underactuated finger and rigid thumb (*64*), prioritizing in-hand manipulation and the stability of grasp. With more active surfaces and fingers, more complicated in-hand manipulations can be achieved (*65*, *66*). However, the need for rollers within the fingers or the finger's supportive skeletal structure for the "conveyor belt" constrains the choice of materials for constructing the fingers, thereby restricting their flexibility. The material properties and deployable nature of GRIP-tape's appendages alleviates these challenges by using the compliant structure of the appendage as the active surface for manipulation.

The tape appendage structure also allows for sensing and haptic feedback during use operation. We have demonstrated sensing and feedback capabilities using the load cell embedded in the angular control beams. The load cell can measure the force applied to the appendage and then the applied force can be calculated. We can map the force reading of the load cell to the force applied to an object anywhere on the appendage as long as the location of the object is known. These capabilities allowed for the development of automatic functions such as searching, measuring (size and location), and gripping using built-in force measurements and structural compliance. Furthermore, the applied force can also be estimated by an operator through visual inspection, as the radius of curvature at the ends of the appendage decreases when the gripping force increases. This could allow a trained operator to judge at a glance how much force is being applied at any given time while teleoperating the GRIP-tape system. That is also why our forward and inverse kinematic model for translating the object includes the curvature at the tip of the appendage as a variable. Unlike previous studies that neglect the curvature at the tip and rely primarily on the axial stiffness of the tape springs rather than bending stiffness (*47*–*49*), our study considers the curvature, which changes with the gripping force. Accounting for this variation is crucial for improving the model's accuracy.

Potential applications for deployable manipulators include agriculture, space, and sea environments. Agriculture remains a challenging environment for robotics as it is unplanned and variable, requiring a capability for adaptation. In addition, for a robot to be adopted on a farm, it must be both low cost and safe around humans (*67*). The GRIP-tape system may find use in agriculture applications where autonomous picking and inspection are required. The tape springs that form the actuated appendages are both cheap to produce and safe to use for human interaction due to their buckling properties. Furthermore, the different actuation modes of the GRIP-tape could be particularly useful in picking applications, for example, reaching out and grabbing a fruit, twisting it off the plant, then retracting and conveying the fruit back to a central body for inspection. While these functions can be also achieved by some previous studies on active surfaces, GRIP-tape offers advantages in soft gripping and reachability. The compliant and spring-like nature of the end joint would allow for force control while harvesting produce and would lower the chance of damaging a fruit while harvesting it. Autonomous detection and measurement can also benefit from the length of the arms, an object can be first approximately located by one or multiple visual sensors and further located by the extended arms.

In addition to agriculture, the lightweight and high extensibility of the GRIP-tape manipulator could be useful in environments where volume and weight are at a premium such as space. Tape springs are already used as for space systems such as antenna booms, satellite solar arrays, and structural supports (*68*, *69*). A tape spring–based actuator could be similarly effective, allowing for highly extensible actuators to be sent on space missions with substantially lower weight and volume than rigid link robots with the same reach distance. Similarly, an extensible gripper could be useful in deep sea environments where space is limited within the vehicle. Sea caves are complex and space limited environments that are interesting places to search for new life (*70*). The narrow constraints of the caves limit the equipment that can be carried inside, motivating the use of actuators that can be packed into a small volume and then extended.

There are areas where the GRIP-tape design could be improved. The convex surface of the tape spring is not an ideal shape for gripping, particularly when only two supporting fingers are used, which limits its ability to grasp objects with sloped or irregular surfaces. Introducing an additional appendage and adopting a triangular layout could substantially expand its manipulation capabilities, enabling better performance with at least one supporting appendage positioned beneath the object. We will also consider applying surface treatments to the tape to further improve gripping stability. Thus, in future research, we may design a three-finger or four-finger manipulator based on the GRIP-tape but with a more stable grip. Another potential direction for future development is to combine two sets of grippers in a perpendicular configuration or three appendages in a triangular arrangement, which would not only provide a more secure grip but also introduce an additional degree of freedom. With more than three active surfaces, where any two can define a rotation axis, the system can generate all possible rotation vectors within a plane. The remaining rotational dimension could be managed by a rotary stage, enabling full 3D rotation. In addition, multiple appendages offer a more stable grip compared to bimanual gripping.

In summary, the deployability and "soft"-mechanics of tape springs presents future opportunities for manipulation robots. Comprehensively, the GRIP-tape is an example of a broader class of soft, curved, reconfigurable, and anisotropic mechanisms that provide a broad repertoire of mechanical properties for soft robot development (*53*, *71*–*73*). The GRIP-tape has been developed with the goal of creating an extensible gripper by utilizing the curvature properties of tape springs. The ease of fabrication and the unique mechanical properties of tape springs make them ideal structures for high extensibility manipulators. Future manipulators based on this concept could be engineered for more advanced object control—including 3D detection, motion, and multi-axis object rotation—by adding additional appendages as supports and active surfaces. Overall, the mechanics of soft, curved materials provide bountiful opportunities for future reconfigurable robotic mechanisms.

MATERIALS AND METHODS

In this section, we describe in brief the design and fabrication of the GRIP-tape system. Please refer to the Supplementary Materials for more details.

Downloaded from https://www.science.org at University of California San Diego on April 23, 2025

Fabrication

The fabrication setup, illustrated in fig. S1A, mirrors the design mentioned in the mechanism design section, using a 450 mm–by–200 mm acrylic base to house fixed and movable extruders. Two extruders on the far left and right directly manage the appendages' supporting sections, while two central extruders, positioned on a track, are guided by a rack-and-pinion mechanism for precise linear motion. This motion is stabilized by two 8-mm metal rods serving as guiding tracks, with smooth travel facilitated by linear bearings (fig. S1B). The system is powered by seven DYNAMIXEL motors, including five XL430-W250-T units for length and gap control of the appendages and two XM540-W270-T motors for angular adjustments.

The extruder design incorporates active and passive rollers mounted on shafts supported by 5 mm–by–10 mm–by–4 mm bearings, with sandpaper-coated rollers enhancing friction. Each extruder includes entrance and exit guides designed to accommodate tape deformation, ensuring uniform support and preventing undesired bends caused by compression or external forces (fig. S1D). For angular control, the unit features a guiding ring mounted 115 mm away from the motor axis, with an offset rotational axis to minimize collisions between the beam and tape during movement. An "X"-shaped stabilizer further supports the guiding ring, ensuring the tape remains upright in section view, contributing to improved gripping performance (fig. S1E). Additional construction details can be found in the Supplementary Materials.

Motion programming

The programming framework for GRIP-tape, developed using MATLAB and DYNAMIXEL Protocol 2.0, enables precise control and real-time feedback for the gripper's movement and configuration (figs. S4 to S7). The system coordinates seven DYNAMIXEL motors using built-in proportional-integral-derivative controllers and a load cell for force feedback. Basic functions include forward kinematics for appendage positioning and modes for appendage transformation: Tip remain mode maintains consistent contact geometry, Outer only mode adjusts outer appendages for object manipulation without angular displacement, and inner only mode exclusively moves central extruders along the track.

For object gripping and manipulation, the program adjusts the distance between inner extruders to ensure parallel contact for equalized gripping forces. Translation combines gripping with appendage transformations along calculated waypoints, minimizing mid-way drops caused by nonlinear forward kinematics. Object rotation and conveying are achieved by synchronized appendage motions, where same-direction movements induce object rotation, while opposite-direction movements enable conveyance.

We developed a MATLAB-based app enhances usability, featuring sliders for position and force control, real-time appendage layout visualization, and emergency stops. An "Auto" function integrates object detection, measurement, and gripping. Gamepad controls (Logitech F310) further facilitate manual adjustments, enabling intuitive manipulation of location, gap, and gripping force, along with object rotation and conveying functionalities. For more technical implementation details, see the Supplementary Materials.

Mechanical testing

We used two experimental setups to characterize the mechanical behavior of the tape spring appendages. The first setup, a MARK-10 ESM750S Motorized Tension/Compression Test Stand with a MARK-10 M7-20 force gauge, was used to evaluate the three-point bending strength of various tape configurations and the stiffness of the appendage's tip curve. This setup allowed precise measurement of loading versus displacement curves.

The second setup focused on measuring the buckling strength and durability of the appendages. It consisted of a rotational stepper motor (SOYO SY42STH38-1684A), a rotary stage (Parker 30005-S), a load cell (YZC-133 1KG), and an amplifier (FUTEK IAA100). In this experiment, the straightened appendage was mounted on the rotary stage driven by the stepper motor and rotated into contact with a fixed-load cell at defined distances, providing data on the appendage's resistance to buckling and its performance under repeated loading.

Kinematics experiment

The accuracy of the GRIP-tape appendage control was evaluated using a motion capture software OptiTrack Motive and OptiTrack Primex 13 cameras. We performed two sets of experiments to characterize the theoretical kinematics model compared to the actual appendage motion. In the first experiment, we commanded the appendage to move to 16 locations across a 4×4 grid over the workspace (Fig. 4C), with six trials for each location. In the second experiment, we commanded the appendage tip to move along different *xy* paths over three cycles.

Supplementary Materials

The PDF file includes:
Materials and Methods
Figs. S1 to S10
Legends for movies S1 to S8

Other Supplementary Material for this manuscript includes the following:
Movies S1 to S8

REFERENCES AND NOTES

1. S. Pellegrino, *Deployable Structures* (Springer, 2001).
2. G. E. Fenci, N. G. R. Currie, Deployable structures classification: A review. *Int. J. Space Struct.* **32**, 112–130 (2017).
3. B. Suthar, S. Jung, Design and feasibility analysis of a foldable robot arm for drones using a twisted string actuator: FRAD-TSA. *IEEE Robot. Autom. Lett.* **6**, 5769–5775 (2021).
4. S. Teshigawara, H. Harry Asada, A mobile extendable robot arm: Singularity analysis and design, in *IEEE/RSJ International Conference on Intelligent Robots and Systems (IROS)* (IEEE, 2019), pp. 5131–5138.
5. C. C. Kemp, A. Edsinger, H. M. Clever, B. Matulevich, The design of stretch: A compact, lightweight mobile manipulator for indoor human environments, in *2022 International Conference on Robotics and Automation (ICRA)* (IEEE, 2022), pp. 3150–3157.
6. X. Ding, Y. Yang, J. S. Dai, Design and kinematic analysis of a novel prism deployable mechanism. *Mech. Mach. Theory* **63**, 35–49 (2013).
7. G. Wei, Y. Chen, J. S. Dai, Synthesis, Mobility, and multifurcation of deployable polyhedral mechanisms with radially reciprocating motion. *J. Mech. Des.* **136**, 091003 (2014).
8. Z. You, S. Pellegrino, Foldable bar structures. *Int. J. Solids Struct.* **34**, 1825–1847 (1997).
9. D. Rus, M. T. Tolley, Design, fabrication and control of origami robots. *Nat. Rev. Mater.* **3**, 101–112 (2018).
10. S.-J. Kim, D.-Y. Lee, G.-P. Jung, K.-J. Cho, An origami-inspired, self-locking robotic arm that can be folded flat. *Sci. Rob.* **3**, eaar2915 (2018).
11. S. Wu, Q. Ze, J. Dai, N. Udipi, G. H. Paulino, R. Zhao, Stretchable origami robotic arm with omnidirectional bending and twisting. *Proc. Natl. Acad. Sci. U.S.A.* **118**, e2110023118 (2021).
12. Y. Park, J. Kang, Y. Na, Reconfigurable shape morphing with origami-inspired pneumatic blocks. *IEEE Robot. Autom. Lett.* **7**, 9453–9460 (2022).
13. T. Yan, S. Teshigawara, H. Harry Asada, Design of a growing robot inspired by plant growth, in 2019 *IEEE/RSJ International Conference on Intelligent Robots and Systems (IROS)* (IEEE, 2019), pp. 8006–8011.
14. W. Wang, H. Rodrigue, S.-H. Ahn, Deployable soft composite structures. *Sci. Rep.* **6**, 20869 (2016).

Downloaded from https://www.science.org at University of California San Diego on April 23, 2025

15. J. F. Boudet, J. Lintuvuori, C. Lacouture, T. Barois, A. Deblais, K. Xie, S. Cassagnere, B. Tregon, D. B. Brückner, J. C. Baret, H. Kellay, From collections of independent, mindless robots to flexible, mobile, and directional superstructures. *Sci. Robot.* **6**, eabd0272 (2021).
16. F. Ilievski, A. D. Mazzeo, R. F. Shepherd, X. Chen, G. M. Whitesides, Soft robotics for chemists. *Angew. Chem. Int. Ed. Engl.* **50**, 1890–1895 (2011).
17. J. D. Greer, L. H. Blumenschein, R. Alterovitz, E. W. Hawkes, A. M. Okamura, Robust navigation of a soft growing robot by exploiting contact with the environment. *Int. J. Rob. Res.* **39**, 1724–1738 (2020).
18. A. D. Marchese, C. D. Onal, D. Rus, Autonomous soft robotic fish capable of escape maneuvers using fluidic elastomer actuators. *Soft Robot.* **1**, 75–87 (2014).
19. E. Brown, N. Rodenberg, J. Amend, A. Mozeika, E. Steltz, M. R. Zakin, H. Lipson, H. M. Jaeger, Universal robotic gripper based on the jamming of granular material. *Proc. Natl. Acad. Sci. U.S.A.* **107**, 18809–18814 (2010).
20. K. C. Galloway, K. P. Becker, B. Phillips, J. Kirby, S. Licht, D. Tchernov, R. J. Wood, D. F. Gruber, Soft robotic grippers for biological sampling on deep reefs. *Soft Robot.* **3**, 23–33 (2016).
21. P. Polygerinos, Z. Wang, K. C. Galloway, R. J. Wood, C. J. Walsh, Soft robotic glove for combined assistance and at-home rehabilitation. *Robot. Auton. Syst.* **73**, 135–143 (2015).
22. S. K. Talas, B. A. Baydere, T. Altinsoy, C. Tutcu, E. Samur, Design and development of a growing pneumatic soft robot. *Soft Robot.* **7**, 521–533 (2020).
23. Z. M. Hammond, N. S. Usevitch, E. W. Hawkes, S. Follmer, Pneumatic Reel Actuator: Design, modeling, and implementation, in *2017 IEEE International Conference on Robotics and Automation (ICRA)* (IEEE, 2017), pp. 626–633.
24. E. W. Hawkes, L. H. Blumenschein, J. D. Greer, A. M. Okamura, A soft robot that navigates its environment through growth. *Sci. Robot.* **2**, eaan3028 (2017).
25. F. Putzu, T. Abrar, K. Althoefer, Plant-Inspired Soft Pneumatic Eversion Robot, in *2018 7th IEEE International Conference on Biomedical Robotics and Biomechatronics (Biorob)* (IEEE, 2018), pp. 1327–1332.
26. J. D. Greer, T. K. Morimoto, A. M. Okamura, E. W. Hawkes, A soft, steerable continuum robot that grows via tip extension. *Soft Robot.* **6**, 95–108 (2019).
27. P. Li, Y. Zhang, G. Zhang, D. Zhou, L. Li, A bioinspired soft robot combining the growth adaptability of vine plants with a coordinated control system. *Research* **2021**, 9843859 (2021).
28. L. H. Blumenschein, L. T. Gan, J. A. Fan, A. M. Okamura, E. W. Hawkes, A tip-extending soft robot enables reconfigurable and deployable antennas. *IEEE Robot. Autom. Lett.* **3**, 949–956 (2018).
29. D.-K. Kim, G.-P. Jung, A highly compact zip chain arm with origami-inspired folding chain structures. *Biomimetics* **8**, 176 (2023).
30. F. Collins, M. Yim, Design of a spherical robot arm with the Spiral Zipper prismatic joint, in *2016 IEEE International Conference on Robotics and Automation (ICRA)* (IEEE, 2016), pp. 2137–2143.
31. A. Sadeghi, A. Mondini, B. Mazzolai, Toward self-growing soft robots inspired by plant roots and based on additive manufacturing technologies. *Soft Robot.* **4**, 211–223 (2017).
32. E. Del Dottore, A. Mondini, N. Rowe, B. Mazzolai, A growing soft robot with climbing plant–inspired adaptive behaviors for navigation in unstructured environments. *Sci. Robot.* **9**, eadi5908 (2024).
33. N. D. Naclerio, A. Karsai, M. Murray-Cooper, Y. Ozkan-Aydin, E. Aydin, D. I. Goldman, E. W. Hawkes, Controlling subterranean forces enables a fast, steerable, burrowing soft robot. *Sci. Robot.* **6**, eabe2922 (2021).
34. L. H. Blumenschein, M. M. Coad, D. A. Haggerty, A. M. Okamura, E. W. Hawkes, Design, modeling, control, and application of everting vine robots. *Front. Robot. AI* **7**, 548266 (2020).
35. M. Jiang, J. Wang, N. Gravish, A reconfigurable soft linkage robot via internal "virtual" joints. *Soft Robot.* **11**, 946–957 (2024).
36. C. Sickinger, L. Herbeck, T. Ströhlein, J. Torrez-Torres, in *55th International Astronautical Congress of the International Astronautical Federation, the International Academy of Astronautics, and the International Institute of Space Law* , International Astronautical Congress (IAF) (American Institute of Aeronautics and Astronautics, 2004).
37. H. M. Y. C. Mallikarachchi, S. Pellegrino, Deployment dynamics of ultrathin composite booms with tape-spring hinges. *J. Spacecr. Rockets* **51**, 604–613 (2014).
38. M. Leipold, C. Sickinger, H. Runge, Large SAR membrane antennas with lightweight deployable booms, in *Proceedings of the 28th ESA Antenna Workshop on Space Antenna Systems and Technologies* (ESA, 2005).
39. T. Murphey, S. Jeon, A. Biskner, G. Sanford, Deployable booms and antennas using bi-stable tape-springs, in *Proceedings of the 24th Annual AIAA/USU Conference on Small Satellites* (DigitalCommons@USU, 2010). Mission Enabling Technologies, SSC10-X-6, https://digitalcommons.usu.edu/smallsat/2010/all2010/58/
40. S. Seriani, P. Gallina, A storable tubular extendible member (STEM) parallel robot: Modelization and evaluation. *Mech. Mach. Theory* **90**, 95–107 (2015).
41. T. Ding, B. Li, H. Liu, Y.-N. Peng, Y. Yang, Planar multi-closed-loop hyper-redundant manipulator using extendable tape springs: Design, modeling, and experiments. *IEEE Robot. Autom. Lett.* **7**, 6630–6637 (2022).
42. K. Seffen, S. Pellegrino, Deployment of a rigid panel by tape-springs (Springer, 1997).
43. T. G. Chen, S. Newdick, J. Di, C. Bosio, N. Ongole, M. Lapotre, M. Pavone, M. R. Cutkosky, Locomotion as manipulation with ReachBot. *Sci. Robot.* **9**, eadi9762 (2024).
44. T. G. Chen, B. Miller, C. Winston, S. Schneider, A. Bylard, M. Pavone, M. R. Cutkosky, ReachBot: A Small Robot with Exceptional Reach for Rough Terrain, in *2022 International Conference on Robotics and Automation (ICRA)* (IEEE, 2022), pp. 4517–4523.
45. S. Schneider, A. Bylard, T. G. Chen, P. Wang, M. R. Cutkosky, and M. Pavone, ReachBot: A small robot for large mobile manipulation tasks, in *2022 IEEE Aerospace Conference*, (IEEE, 2022), pp. 1–12.
46. S. Newdick, T. G. Chen, B. Hockman, E. Schmerling, M. R. Cutkosky, M. Pavone, Designing ReachBot: System design process with a case study of a Martian lava tube mission, in *2023 IEEE Aerospace Conference*, (IEEE, 2023), pp. 1–9.
47. H. Liu, Y. Qin, Y. Yang, Structure design and kinematic performance of the deployable translational parallel tape-spring manipulator. *Robotica* **42**, 1523–1548 (2024).
48. Y. Yang, Y. Qin, Y. Tang, Y. Yang, Y. Peng, H. Pu, Deployable closed-loop tape-spring manipulators with mobile drive components on localized folds. *Mech. Mach. Theory* **167**, 104553 (2022).
49. T. Yaqi, H. Zheng, T. Lei, P. Yan, P. Huayan, Y. Yang, Design of a lightweight deployable planar parallel manipulator with tape spring mechanism, in *Proceedings of the 4th International Workshop on Fundamental Issues, Applications and Future Research Directions for Parallel Mechanisms /Manipulators / Machines* (2020).
50. J. Quan, D. Hong, Extending and bending robotic limbs using tape springs for mobility and manipulation: Preliminary investigations, in *Proceedings of the ASME 2022 International Design Engineering Technical Conferences and Computers and Information in Engineering Conference,* (ASME, 2022).
51. J. Quan, D. Hong, Flexible long-reach robotic limbs using tape springs for mobility and manipulation. *J. Mech. Robot.* **15**, 031009 (2023).
52. O. Godson Osele, A. M. Okamura, B. H. Do, A lightweight, high-extension, planar 3-degree-of-freedom manipulator using pinched bistable tapes, in *2022 International Conference on Robotics and Automation (ICRA)* (IEEE, 2022), pp. 1190–1196.
53. C. Sparks, N. Jutus, R. Hatton, N. Gravish, Amoeba-inspired swimming through isoperimetric modulation of body shape, in *IEEE International Conference on Intelligent Robots and Systems (IROS)* (IEEE, 2022), pp. 2685–2692.
54. O. T. Abdoun, M. Yim, Assessing tissue damage around a tape spring steerable needle with sharp turn radii, in *IEEE Open Journal of Engineering in Medicine and Biology*, vol. 5, pp. 45-49, (2024).
55. J. M. Fernandez, Advanced deployable Shell-Based composite booms for small satellite structural applications including solar sails (Tech. Rep. NF1676L-25486, 2017).
56. Ö. Soykasap, Analysis of tape spring hinges. *Int. J. Mech. Sci.* **49**, 853–860 (2007).
57. C. R. Calladine, The Theory of thin shell structures 1888–1988. *Proc. Inst. Mech. Eng. Part A* **202**, 141–149 (1988).
58. Y. Kim, G. A. Parada, S. Liu, X. Zhao, Ferromagnetic soft continuum robots. *Sci. Robot.* **4**, eaax7329 (2019).
59. N. S. Usevitch, Z. M. Hammond, M. Schwager, A. M. Okamura, E. W. Hawkes, S. Follmer, An untethered isoperimetric soft robot. *Sci Robot* **5**, eaaz0492 (2020).
60. A. Kakogawa, H. Nishimura, *S. Ma*, Underactuated modular finger with pull-in mechanism for a robotic gripper, in *2016 IEEE International Conference on Robotics and Biomimetics (ROBIO)* (IEEE, 2016), pp. 556–561.
61. K. Morino, S. Kikuchi, S. Chikagawa, M. Izumi, T. Watanabe, Sheet-based gripper featuring passive pull-in functionality for bin picking and for picking up thin flexible objects. *IEEE Robot. Autom. Lett.* **5**, 2007–2014 (2020).
62. V. Tincani, M. G. Catalano, E. Farnioli, M. Garabini, G. Grioli, G. Fantoni, and A. Bicchi, Velvet fingers: A dexterous gripper with active surfaces, in *Proceedings of the IEEE/RSJ International Conference on Intelligent Robots and Systems* (IEEE, 2012), pp. 1257–1263.
63. R. Krug, T. Stoyanov, M. Bonilla, V. Tincani, N. Vaskevicius, G. Fantoni, A. Birk, A. Lilienthal, A. Bicchi, Velvet fingers: Grasp planning and execution for an underactuated gripper with active surfaces, in *2014 IEEE International Conference on Robotics and Automation (ICRA)* (IEEE, 2014), pp. 3669–3675.
64. R. R. Ma, A. M. Dollar, In-hand manipulation primitives for a minimal, underactuated gripper with active surfaces, *ASME 2016 International Design Engineering Technical Conferences and Computers and Information in Engineering Conference* (ASME, 2016), p. V05AT07A072.
65. Y. Cai, S. Yuan, In-hand manipulation in power grasp: Design of an adaptive robot hand with active surfaces, in *2023 IEEE International Conference on Robotics and Automation (ICRA)* (IEEE, 2023), pp. 10296–10302.
66. G. Xie, R. Holladay, L. Chin, D. Rus, In-hand manipulation with a simple belted parallel-jaw gripper. *IEEE Robot. Autom. Lett.* **9**, 1334–1341 (2024).
67. A. Bechar, C. Vigneault, Agricultural robots for field operations: Concepts and components. *Biosys. Eng.* **149**, 94–111 (2016).
68. K. A. Seffen, Z. You, S. Pellegrino, Folding and deployment of curved tape springs. *Int. J. Mech. Sci.* **42**, 2055–2073 (2000).
69. K. Wilkie, The NASA advanced composite solar sail system (ACS3) flight demonstration: A technology pathfinder for practical smallsat solar sailing, in *Proceedings of the 35th*

Downloaded from https://www.science.org at University of California San Diego on April 23, 2025

Annual AIAA/USU Conference on Small Satellites (DigitalCommons@USU, 2021). Next on the Pad, SSC21-II-10, https://digitalcommons.usu.edu/smallsat/2021/all2021/146/
70. K. Richmond, C. Flesher, N. Tanner, V. Siegel, W. C. Stone, Autonomous exploration and 3-D mapping of underwater caves with the human-portable SUNFISH® AUV, in *Global Oceans 2020: Singapore - U.S. Gulf Coast* (IEEE, 2020), pp. 1–10.
71. M. Jiang, Q. Yu, N. Gravish, Vacuum induced tube pinching enables reconfigurable flexure joints with controllable bend axis and stiffness, in *2021 IEEE 4th International Conference on Soft Robotics (RoboSoft)* (IEEE, 2021), pp. 315–320.
72. M. Sharifzadeh, Y. Jiang, D. M. Aukes, Reconfigurable curved beams for selectable swimming gaits in an underwater robot. *IEEE Robot. Autom. Lett.* **6**, 3437–3444 (2021).
73. Y. Jiang, M. Sharifzadeh, D. M. Aukes, Reconfigurable Soft Flexure Hinges via Pinched Tubes, in *IEEE/RSJ International Conference on Intelligent Robots and Systems (IROS)* (IEEE, 2020), pp. 8843–8850.

Acknowledgments: We acknowledge D. Aukes, R. Hatton, and C. Harnett for helpful discussion. We also acknowledge D. Li for the help with recording robot arm demonstrations. **Funding:** Funding support was provided through the Mechanical and Aerospace Engineering Department at UCSD. This material was based on work supported by the National Science Foundation under grant no. 1935324 and the Office of Naval Research under grant number N00014-20-1-2373. Any opinions, findings, and conclusions, or recommendations expressed in this material are those of the author(s) and do not necessarily reflect the views of the National Science Foundation. **Author contributions:** Conceptualization: G.H., C.S., and N.G. Methodology: G.H., C.S., and N.G. Investigation: G.H. and C.S. Visualization: G.H. Supervision: N.G. Writing—original draft: G.H., C.S., and N.G. Writing—review and editing: G.H., C.S., and N.G. **Competing interests:** G.H., C.S., and N.G. are co-inventors on a provisional patent filed by the University of California San Diego titled "Tape spring mechanisms for deployable manipulation", under US Provisional Application Serial No. 63/566,799 filed 18 March 2024. The authors declare that they have no other competing interests. **Data materials and availability:** All data needed to evaluate the conclusions in the paper are present in the paper and/or the Supplementary Materials.

Submitted 2 October 2024
Accepted 5 March 2025
Published 9 April 2025
10.1126/sciadv.adt5905

Downloaded from https://www.science.org at University of California San Diego on April 23, 2025